Title

Development and validation of a measurement-based source model for kilovoltage cone-beam CT Monte Carlo dosimetry simulations.

Journal

Medical Physics, 40(11)

Authors

McMillan, Kyle
Mcnitt-Gray, Michael
Ruan, Dan

Publication Date

2013-11-01

DOI

10.1118/1.4823795

Peer reviewed

Development and validation of a measurement-based source model for kilovoltage cone-beam CT Monte Carlo dosimetry simulations

Kyle McMillan[a)]
Department of Biomedical Physics, David Geffen School of Medicine, University of California, Los Angeles, Los Angeles, California 90024

Michael McNitt-Gray
Department of Biomedical Physics and Department of Radiology, David Geffen School of Medicine, University of California, Los Angeles, Los Angeles, California 90024

Dan Ruan
Department of Biomedical Physics and Department of Radiation Oncology, David Geffen School of Medicine, University of California, Los Angeles, Los Angeles, California 90024

(Received 10 June 2013; revised 26 August 2013; accepted for publication 16 September 2013; published 10 October 2013)

Purpose: The purpose of this study is to adapt an equivalent source model originally developed for conventional CT Monte Carlo dose quantification to the radiation oncology context and validate its application for evaluating concomitant dose incurred by a kilovoltage (kV) cone-beam CT (CBCT) system integrated into a linear accelerator.
Methods: In order to properly characterize beams from the integrated kV CBCT system, the authors have adapted a previously developed equivalent source model consisting of an equivalent spectrum module that takes into account intrinsic filtration and an equivalent filter module characterizing the added bowtie filtration. An equivalent spectrum was generated for an 80, 100, and 125 kVp beam with beam energy characterized by half-value layer measurements. An equivalent filter description was generated from bowtie profile measurements for both the full- and half-bowtie. Equivalent source models for each combination of equivalent spectrum and filter were incorporated into the Monte Carlo software package MCNPX. Monte Carlo simulations were then validated against in-phantom measurements for both the radiographic and CBCT mode of operation of the kV CBCT system. Radiographic and CBCT imaging dose was measured for a variety of protocols at various locations within a body (32 cm in diameter) and head (16 cm in diameter) CTDI phantom. The in-phantom radiographic and CBCT dose was simulated at all measurement locations and converted to absolute dose using normalization factors calculated from air scan measurements and corresponding simulations. The simulated results were compared with the physical measurements and their discrepancies were assessed quantitatively.
Results: Strong agreement was observed between in-phantom simulations and measurements. For the radiographic protocols, simulations uniformly underestimated measurements by 0.54%–5.14% (mean difference = −3.07%, SD = 1.60%). For the CBCT protocols, simulations uniformly underestimated measurements by 1.35%–5.31% (mean difference = −3.42%, SD = 1.09%).
Conclusions: This work demonstrates the feasibility of using a measurement-based kV CBCT source model to facilitate dose calculations with Monte Carlo methods for both the radiographic and CBCT mode of operation. While this initial work validates simulations against measurements for simple geometries, future work will involve utilizing the source model to investigate kV CBCT dosimetry with more complex anthropomorphic phantoms and patient specific models. © *2013 American Association of Physicists in Medicine*. [http://dx.doi.org/10.1118/1.4823795]

Key words: OBI, CBCT, radiation dose, Monte Carlo dose simulations

1. INTRODUCTION

Modern radiotherapy utilizes image guidance intensively. Radiograph-based techniques [radiographic, fluoroscopic, cone-beam CT (CBCT)] are popular choices, with the convenience of integrated kilovoltage (kV) imaging devices and interfaces offered with many commercial treatment systems. While the dose impact of these imaging procedures has often been regarded as negligible when compared with the intended therapy dose, continuous imaging and a greater attention to the dose to areas outside of the target volume have raised concerns of concomitant imaging dose.[1–3] This invites a systematic approach to accurately quantify the dose impact of imaging in the context of radiotherapy.[4,5]

Monte Carlo techniques are readily employed to accurately simulate the dose from radiation transport.[6] The accuracy of Monte Carlo techniques in the area of CT dosimetry is well established.[7–11] More recently, Monte Carlo techniques have been used to simulate the dose from the kV imagers integrated into linear accelerators, such as the On-Board Imager (OBI)

integrated into the Trilogy accelerator (Varian Medical Systems, Palo Alto, CA).[12–15] In order to generate an accurate Monte Carlo simulation of the OBI dose, detailed information about the x-ray spectrum, internal filtration, added bowtie filtration and beam geometry (i.e., focal spot to isocenter distance, cone angle, and collimation) is needed. While much of this information can be referenced from OBI documentation, some of the information, such as energy spectra and bowtie filter descriptions may be proprietary and therefore only be obtained from the manufacturer under a nondisclosure agreement. Using manufacturer data to construct a Monte Carlo model can be a laborious process, with the need to describe each component of the model in great detail. Additionally, proprietary data from the vendors provide information about their "reference" machine that may differ slightly from the specific system that is to be characterized.

Motivated by a novel measurement-based method developed for conventional CT dose calculation and simulation,[16] this project aims to simplify the OBI Monte Carlo model development process and incorporate into the model machine-specific characteristics by adapting an equivalent source model to the radiotherapy integrated imaging context. The equivalent source model is made up of an equivalent spectrum module and equivalent filter module. The goal of the equivalent spectrum module is to generate an x-ray spectrum, for each beam energy of interest, that is characterized by "equivalent" properties of the original spectrum, which in this case would be the half-value layer (HVL) value obtained experimentally.[17] The goal of the equivalent filter module is to generate a description of the full- and half-bowtie filter that attenuates the equivalent spectrum in the same manner that the actual bowtie filter attenuates the actual spectrum by measuring the variation of bowtie filtration across the x-ray beam. This equivalent source can then be deployed in Monte Carlo simulation tools to estimate radiation doses from OBI imaging.

We will present the development of the OBI equivalent source model and apply it for a variety of beam energies and bowtie filter configurations. To assess the accuracy of the proposed approach, validation studies, based on physical measurements, are performed for a range of beam energies with both full- and half-bowtie filters using both the radiographic and CBCT mode of operation.

2. MATERIALS AND METHODS

2.A. Varian OBI system

The OBI kV imaging system integrated into the Varian Novalis Tx radiosurgery platform (Varian Medical Systems, Palo Alto, CA) was used to produce the kV beams characterized in this investigation. Beam energies from this device range from 40 to 150 kVp. The focal-spot-to-machine-isocenter distance is 100 cm at which the maximum field size is 50 × 50 cm. The beam is collimated by two sets of adjustable lead blades, known as the X-Y blades. The OBI system supports both full-fan and half-fan modes. The former is normally employed for objects with diameters less than 24 cm (i.e., head) while the latter is traditionally used when objects exceed 24 cm in diameter (i.e., pelvis). In the half-fan mode, the flat panel detector is shifted laterally so that an increased field-of-view can be obtained. After the x-ray window, additional filtration in the form of a bowtie filter is used to improve image quality and reduce skin dose. Two bowtie filter options, full-bowtie and half-bowtie, are used with the full- and half-fan modes, respectively. The bowties are shaped in the direction parallel to the anode-cathode direction of the x-ray tube and uniform in thickness in the other direction. Each bowtie has a central thickness of 1.5 cm of aluminum.[12] Figure 1 shows a schematic of the full- and half-fan geometry with the appropriate bowtie filters. The OBI has three modes of kV imaging: radiographic, CBCT, and fluoroscopic. This investigation is focused on the radiographic and CBCT imaging capabilities of the OBI. Radiographic images can be acquired with the imager in the anterior-posterior (AP) or lateral position with respect to the patient (positioned head first, supine). CBCT images can be acquired as either a full- or partial-scan. When the full-fan mode is utilized, a 204° partial-scan (approximately 180° plus the fan angle) is acquired.[14] When objects exceed the 24 cm limit for use of the full-fan mode, the half-fan mode is employed, and a full-scan of 364° (360° + 4° overscan) is acquired.

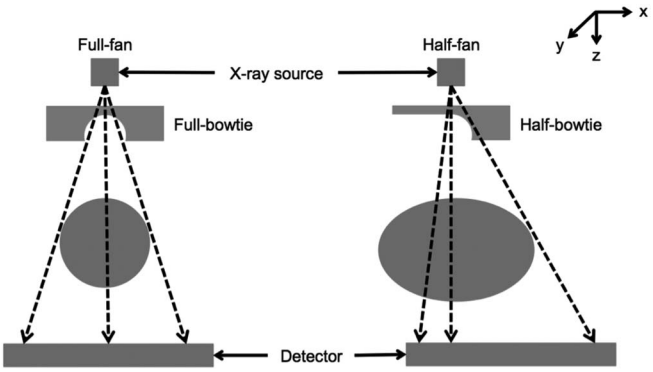

FIG. 1. Full- and half-fan geometry with the appropriate bowtie filters.

2.B. Equivalent source model measurement scheme

2.B.1. Equivalent spectrum module measurements

HVL measurements were made for all beam energies of interest in this investigation. The gantry was rotated such that the therapy head was at the 3 o'clock position and the kV source was at the 12 o'clock position. All added bowtie filters were removed, and a 0.6 cm^3 thimble ionization chamber (Model 10X5-0.6, Radcal Corporation, Monrovia, CA) was attached to the treatment table such that the active portion of the chamber was extended beyond the edge of the table at the machine isocenter. The thimble ionization chamber was calibrated against a secondary diagnostic energy standard traceable to a primary standard. Table I shows the technical settings used to make the HVL measurements. The X-Y blades were set to 5 cm × 5 cm for a narrow beam measurement. An initial exposure was made at isocenter using the

TABLE I. Technical settings for HVL and bowtie profile measurements.

	HVL measurements	Bowtie profile measurements
X-ray voltage (kVp)	80, 100, 125	125
X-ray current (mA)	200	250
X-ray milliseconds (ms)	500	2500
Exposure (mAs)	100	625
Blade X1 (cm)	2.5	25.0
Blade X2 (cm)	2.5	25.0
Blade Y1 (cm)	2.5	25.0
Blade Y2 (cm)	2.5	25.0

radiographic mode of operation of the OBI. Subsequent exposures were made at isocenter using incremental thicknesses of high-purity (99.9%) aluminum (Al) placed 50 cm from the ionization chamber until the resultant exposure was less than one-half the initial exposure.

2.B.2. Equivalent Bowtie filter module measurements

Bowtie profile measurements were made for both the full- and half-bowtie filter. The gantry was rotated such that the therapy head was at the 6 o'clock position and the kV source was at the 3 o'clock position. The bowtie filter to be profiled was attached to the x-ray window, and the 0.6 cm^3 thimble ionization chamber used in the HVL measurements was attached to the treatment table, with the table outside the direct x-ray beam path, and placed at the machine isocenter. The full profile (across the entire field of view) was obtained. Table I shows the technical settings used to make the bowtie profile measurements. Because there exists only one full-bowtie and one half-bowtie for the current OBI device, a single description of each bowtie was generated by making profile measurements only for the highest beam energy in this study (125 kVp). The X-Y blades were set to the maximum field size of 50 × 50 cm to profile the entire field under influence of the bowtie filters. An initial exposure was made at isocenter, and subsequent exposures were made by moving the treatment table in 5 mm increments in the ±z-direction to obtain the entire profile of exposure attenuations from the bowtie filter as a function of the ray angle. Figure 2 shows the experimental setup for the bowtie profile measurements.

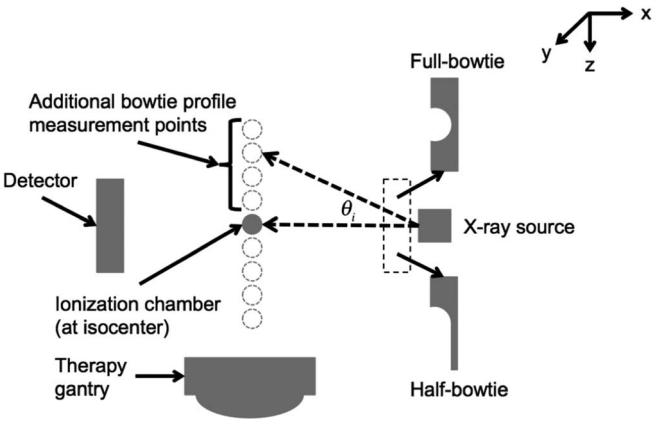

FIG. 2. Experimental setup for the bowtie profile measurements.

2.C. Equivalent source model computational methods

2.C.1. Equivalent spectrum module computation

The equivalent source model is made up of two components, the first of which is the equivalent spectrum module. The goal of the equivalent spectrum module is to generate an x-ray photon spectrum with a calculated beam behavior that best matches key characteristics of the OBI system; specifically, the equivalent spectrum is chosen based on matching the HVL value measured experimentally, and in doing so takes into account the spectrum off the anode and any inherent filtration of the system (including the housing). Consistent with (1)–(3) in Fig. 3, the following steps are necessary to execute this module:

(1) An initial tungsten (W) spectrum is transmitted through a thin, uniform layer of arbitrarily defined intrinsic filtration material. Assuming exponential attenuation, the number of remaining x-rays at each energy is calculated to produce a candidate spectrum. The initial W spectrum is obtained using a computational tool by Siewerdsen *et al.* called SPEKTR that utilizes Boone and Seibert's tungsten anode spectral model using interpolating polynomials (TASMIP) to obtain spectra with an energy resolution of 1.0 keV for a specified kVp.[18,19]
(2) Using the candidate spectrum, kerma in air is calculated. kerma in air is calculated by summing the product of the energy fluence and the mass energy-transfer coefficient of air $(\mu_{tr}/\rho)_{air}$ over all energies present in the candidate spectrum. For energies in the diagnostic range (20–150 keV) and for low-Z absorbers such as air, the amount of radiative losses is relatively small, so the mass energy-transfer coefficient is approximately equal to the mass energy-absorption coefficient $(\mu_{tr}/\rho)_{air} \cong (\mu_{en}/\rho)_{air}$. Therefore, because they can be easily referenced from numerous sources, mass energy-absorption coefficients are used in the calculation of kerma in air. The mass energy-absorption coefficients used in this investigation are referenced from Hubbell and Seltzer.[20]
(3) The spectrum and subsequent kerma in air resulting from transmitting the candidate spectrum through a thin, uniform thickness of Al is calculated. This step is repeated while incrementally increasing the thickness of Al until the kerma in air is one-half the initial kerma in air calculated in step (2). Because kerma in air is directly proportional to exposure, this thickness of Al represents the calculated HVL of the candidate spectrum.

Steps (1)–(3) are repeated while incrementally increasing the thickness and type of the intrinsic filtration material until the difference between the measured and calculated HVL is

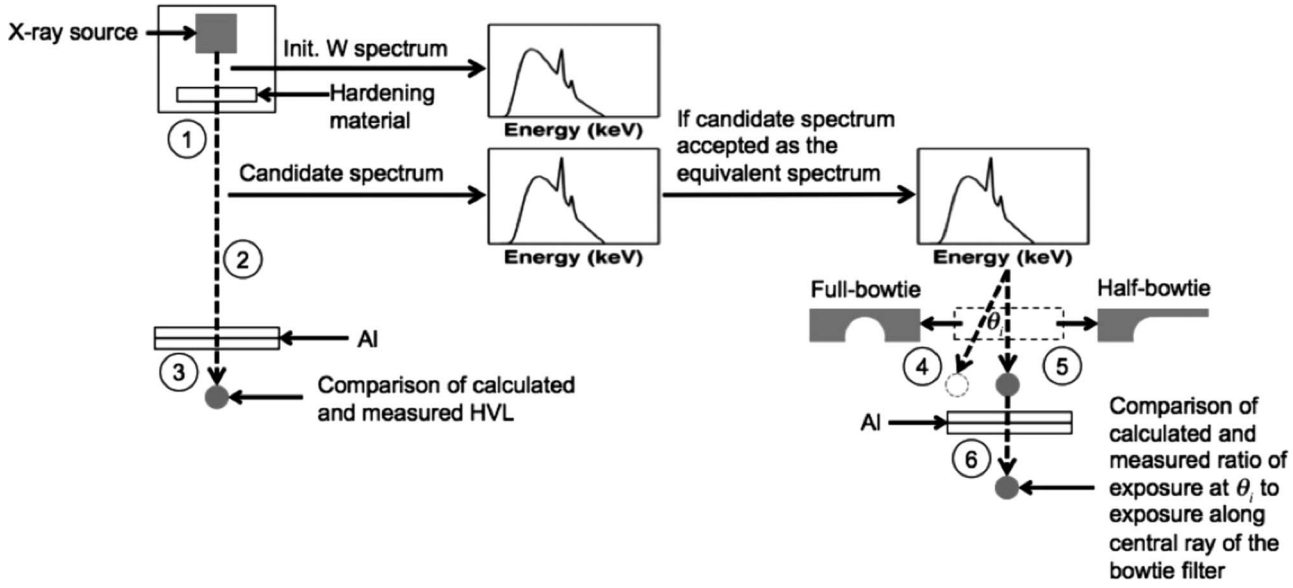

FIG. 3. Diagram of method for generating an equivalent source model using the equivalent spectrum module (Steps 1–3) and the equivalent filter module (Steps 4–6).

minimized. Because this method assumes the exact material composition and design of the filtration scheme is unknown, filtration materials commonly found in x-ray housing construction, including aluminum, graphite, lead, and titanium, were examined as candidates for the equivalent filter material in step (1). The candidate spectrum with the calculated HVL that best matches the measured value (lowest percent difference between the calculated HVL of the candidate spectrum and the measured HVL) is considered the equivalent spectrum. By generating equivalent spectra instead of simply using the basic spectra from SPEKTR, we are able to model the inherent filtration within the x-ray tube housing and include it within the model.

2.C.2. Equivalent Bowtie filter module computation

The second component of the equivalent source model is the equivalent bowtie filter module. The goal of the equivalent filter module is to generate a description of the attenuation profile of the full- and half-bowtie filter such that the equivalent filter attenuates the equivalent spectrum in the same manner that the actual bowtie filter attenuates the x-ray source spectrum. Consistent with (4)–(6) in Fig. 3, the following steps are necessary to execute this module:

(4) Based on the data acquired form the bowtie filter profile measurements, the ratio of the exposure obtained at each angle, θ_i, to the exposure obtained along the central ray of the bowtie filter is calculated.
(5) The equivalent spectrum resulting from the equivalent spectrum module is transmitted through a thickness of bowtie filter material deemed to be the center of the equivalent bowtie filter, and the resultant kerma in air is calculated. The equivalent bowtie filter is arbitrarily assumed to be composed of Al with a central ray thickness of 1.5 cm. The central ray thickness assumption is based upon information available in the literature.[12] While Al may not be the actual material of the actual bowtie filter, this assumption will be shown to be reasonably robust for this approach.
(6) The equivalent spectrum is transmitted through a thickness of Al, and the subsequent kerma in air is calculated. This step is repeated while incrementally increasing the thickness of Al until the difference between the ratio obtained in step (4) and the ratio of the kerma in air through the thickness of Al to the kerma in air from step (5) is minimized. The thickness of Al that minimizes this difference is considered the equivalent path for θ_i.

Steps (4)–(6) are repeated for each angle measured as part of the bowtie filter profile measurement. Combining the equivalent Al path lengths as a function of measured angle produced an equivalent filter description.

2.D. Monte Carlo simulations

The computational results of the equivalent spectrum and bowtie filter modules were incorporated into the Monte Carlo software package MCNPX (Monte Carlo N-Particle eXtended version 2.7.a).[21] Modification was made to the standard MCNPX source code in order to appropriately model the possible x-ray source position, energy, initial trajectory, and attenuation due to the bowtie filter for a variety of OBI radiographic and CBCT protocols.

First, the photon's initial energy is randomly selected from an energy cumulative distribution function created for the equivalent spectrum of interest. Next, the initial position of the photon is selected at a focal-spot-to-machine-isocenter distance of 100 cm. For simulations of the radiographic mode of operation, the initial position is fixed, but for simulations of the CBCT mode of operation, the initial position is

randomly selected from all possible positions for the full- and partial-scan scenarios. An acceptable fan angle and longitudinal beam width (i.e., cone angle) value is then randomly sampled. The direction of the photon is specified by the components of a unit vector in a direction randomly selected from the set of all possible trajectories for a given start position, fan angle, and longitudinal beam width. Finally, attenuation due to the bowtie filter is modeled by adjusting the statistical weighting factor of each photon. The path length of a photon through the bowtie for a given trajectory is linearly interpolated from the bowtie filter description (equivalent Al path length as a function of trajectory angle) generated from the bowtie profile module. Using this path length and the linear attenuation coefficients for Al, the resulting exponential attenuation factor is calculated. Multiplying this exponential attenuation factor by an initial particle weight of 1 yields the new weighting factor for that photon in MCNPX.

Within all the simulations, the detailed photon transport mode with a low-energy cutoff of 1 keV was used. The detailed physics treatment includes coherent scattering and accounts for fluorescent photons after photoelectric absorption. Form factors and Compton profiles are used to account for electron binding effects, and analog capture is always used. The incoherent, coherent, and photoelectric cross section data are based on ENDF/B-IV.[22] Simulation physics options are set so that the photon transport mode does not explicitly create photoelectrons but instead assumes all secondary electrons deposit their energy at the photon interaction site, which is reasonable given the incident photon energy distribution. This assumption satisfies charged particle equilibrium and allows absorbed dose to be approximated as collision kerma, which was calculated in each volume of interest by tallying the photon energy fluence and multiplying by the material-specific and energy-dependent mass energy-absorption coefficient.

2.E. Validation measurements and simulations

2.E.1. Radiographic imaging

Radiographic imaging dose was measured for both a pelvis and head AP protocol. Table II shows the technical settings used to make the radiographic imaging dose measurements. For each radiographic imaging protocol, the x-ray exposure was set to 200 mAs in order to achieve sufficient charge collection within the ionization chamber used to make dose measurements. The desired exposure was achieved by scaling the clinical x-ray exposure time (ms) for each protocol. The pelvis AP protocol utilizes the half-fan mode and a half-bowtie filter while the head AP protocol utilizes the full-fan mode and a full-bowtie filter.

For the pelvis AP protocol, measurements were made with a body (32 cm diameter) CTDI phantom. For the head AP protocol, measurements were made with head (16 cm diameter) CTDI phantom. Each of these homogeneous, polymethyl methacrylate (PMMA) cylindrical phantoms is 15 cm in length and contains one central and four peripheral cylindrical holes the length of the phantom that can be probed by an ionization chamber. The central reference point of the phantom was aligned at machine isocenter, and point dose measurements were made by changing the ionization chamber position among the midpoint of the cylindrical holes under repetitive scans. All measured exposures in milliroentgen (mR) were converted to dose to air in mGy using 1 mR = 0.00876 mGy. Figure 4 shows a cross-sectional schematic of both the body and head CTDI phantoms with each measurement location labeled numerically. The CTDI phantoms, treatment table, and ionization chamber (chamber walls, active volume of air, electrode, etc.) were explicitly modeled using standard geometry and material descriptions in MCNPX, and in-phantom dose was then simulated at all measurement locations by tallying within a 0.6 cm^3 volume of air modeled to represent the active portion of the chamber.

TABLE II. Technical settings for radiographic and CBCT imaging dose measurements. For the Pelvis AP and Head AP radiographic imaging protocols, the x-ray exposure was scaled for measurement by scaling the clinical x-ray exposure time. The clinical exposures and exposure times are given in brackets [].

	Pelvis AP	Head AP	Pelvis CBCT	Standard-dose head CBCT
X-ray voltage (kVp)	80	100	125	100
X-ray current (mA)	200	200	80	20
X-ray milliseconds (ms)	1000 [50]	1000 [40]	13	20
Gantry rotation range (deg)	Fixed	Fixed	364	204
Number of projections	1	1	655	360
X-ray exposure (mAs)	200 [10]	200 [8]	681	144
Fan type	Half	Full	Half	Full
Bowtie filter	Half	Full	Half	Full
Blade X1 (cm)	6.8	13.6	6.8	13.6
Blade X2 (cm)	23.5	13.6	23.5	13.6
Blade Y1 (cm)	10.3	9.2	10.3	9.2
Blade Y2 (cm)	10.3	9.2	10.3	9.2

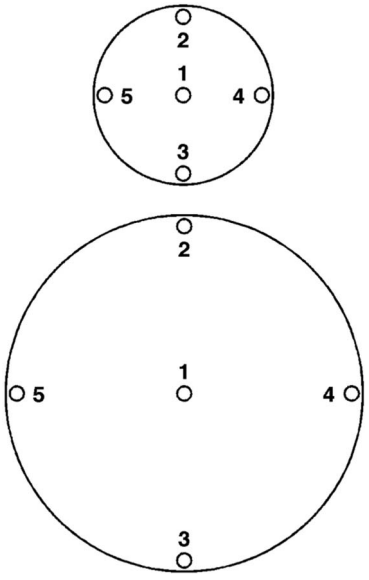

FIG. 4. Cross-sectional schematic of head (top) and body (bottom) CTDI phantom. Measurement locations used in this investigation are labeled numerical.

2.E.2. CBCT imaging

CBCT imaging dose was measured for both a pelvis and standard-dose head CBCT protocol, with the technical settings reported in Table II. According to default clinical settings, images were acquired using the half-fan mode, a half-bowtie filter and a full-scan for the pelvis CBCT protocol and the full-fan mode, a full-bowtie and a partial-scan for the head CBCT protocol. For the partial-scan, images are acquired through 204°. For the full-scan, images are acquired through 364°. The 4° overscan exists on the patient's left lateral. Figure 5 shows a diagram of the partial- and full-scan used in this investigation.

Measurements were made using the body CTDI phantom and the head CTDI phantom for pelvis and head CBCT protocols, respectively. Specific measurement and simulation steps are the same as the radiographic case described in Sec. 2.E.1.

2.F. Comparison of measurements and simulations

Normalization factors are required to convert simulated dose values (mGy per particle) to absolute dose normalized on a tube current time product basis (mGy per mAs) so that direct comparisons can be made between measured and simulated doses. In order to do this, air scan measurements (mGy per mAs) and corresponding simulations (mGy per particle) are performed for all protocols outlined in Table II. Again, measured exposures in mR were converted to dose to air in mGy using 1 mR = 0.00876 mGy. For air scan

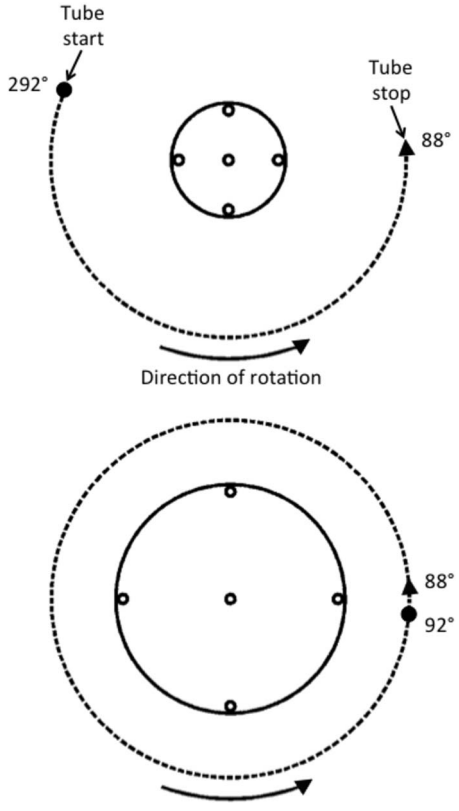

FIG. 5. Diagram of partial- and full-scan. A circle is used to designate the tube start angle and a triangle is used to designate the tube stop angle. For the partial-scan (top), the imager is rotated counter-clockwise through 204° with a starting and stopping angle of 292° and 88°, respectively. For the full-scan (bottom), the imager is rotated counter-clockwise through 364° with the 4° overscan from 92° to 88°.

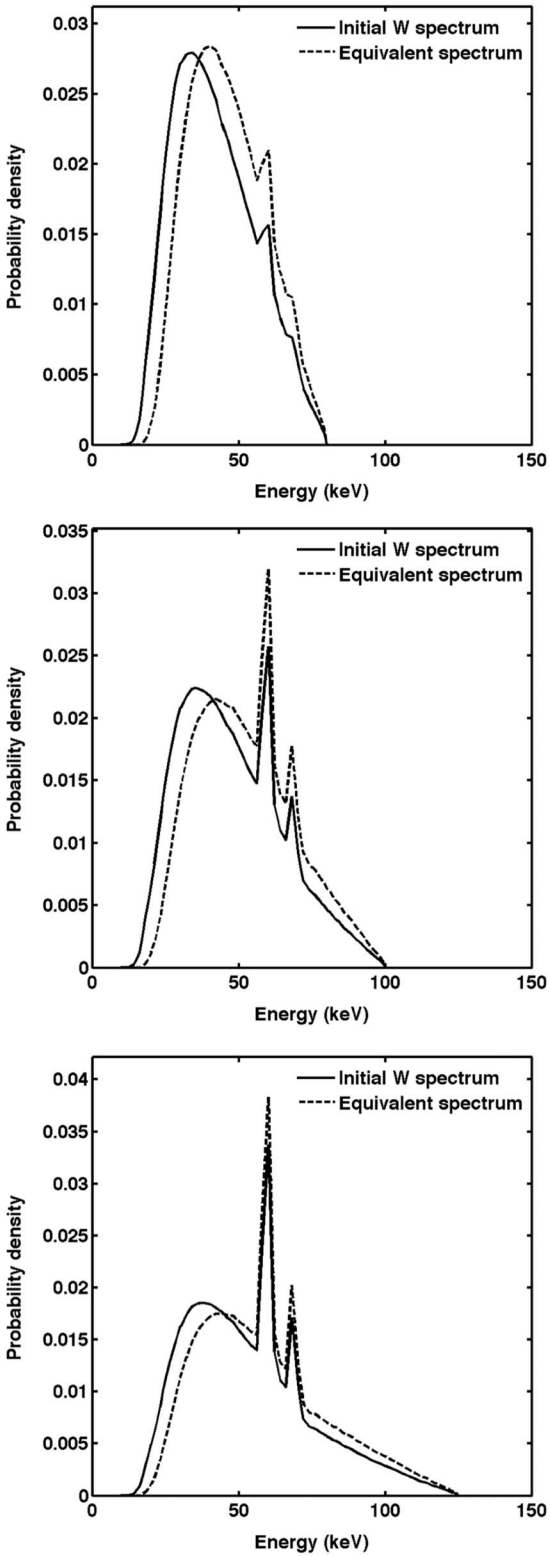

FIG. 6. Probability density functions of the initial W spectrum and the equivalent spectrum for the 80 kVp (top), 100 kVp (middle), and 125 kVp (bottom) scenarios.

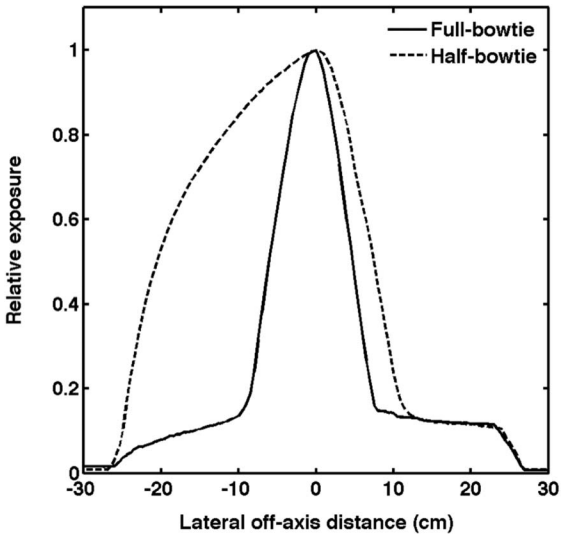

FIG. 7. Bowtie profile measured for both the full- and half-bowtie. Exposures are normalized to the exposure along the central ray of the bowtie filter ($\theta = 0^\circ$).

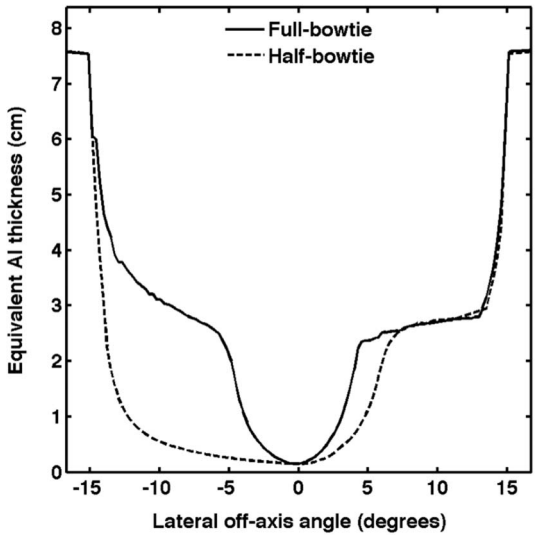

FIG. 8. Equivalent full- and half-bowtie filter generated as part of the equivalent filter module.

measurements, the thimble ionization chamber is attached to the treatment table such that the active portion of the chamber is extended beyond the edge of the table at the machine isocenter and therefore essentially "free-in-air." A corresponding simulation using the ionization chamber model at isocenter is then performed in MCNPX. By dividing the air scan measurement by the air scan simulation, a normalization factor (particle per mAs) is uniquely determined for each protocol, similar to that described by DeMarco *et al.*[23] In-phantom simulations results can then be multiplied by the appropriate normalization factor to yield simulated dose in units of mGy per mAs. Although normalization factors can be calculated using measurements and simulations within some phantom, the advantage of air scan normalization factors is that the chamber position is reproducible in a locally homogeneous dose region void of any nearby attenuating mediums such as the treatment table.[24] Once simulated dose values are properly normalized, percent differences between measurements within the CTDI phantoms and analogous simulations are calculated to access the accuracy of the Monte Carlo model to reproduce in-phantom dose distributions.

3. RESULTS

3.A. Equivalent source model development

The measured HVLs for the 80, 100, and 125 kVp beams are 3.50, 4.34, and 5.41 mm Al, respectively. Equivalent spectrums were developed using these measured HVLs in accordance with the methodology described in Sec. 2.C.1. Figure 6 shows the probability density functions of the initial W spectrum and the estimated equivalent spectrum, characterized by the calculated HVL, for the 80, 100, and 125 keV scenarios.

Figure 7 shows the normalized bowtie profile measured for both the full- and half-bowtie. By incorporating these measurements into the equivalent filter module, equivalent bowtie descriptions were uniquely determined for both the full- and half-bowtie. Figure 8 shows the outputs from the equivalent filter module.

3.B. Radiographic imaging validation

Table III shows the measured and simulated in-phantom dose for the radiographic imaging protocols. For each simulation, 10×10^6 photons histories were used to achieve

TABLE III. Comparison of measured and simulated radiographic imaging dose. Each location is referenced from the diagram in Fig. 4.

	Pelvis AP			Head AP		
Location	Measurement (m Gy/mAs)	MCNPX (mGy/mAs)	% Diff.	Measurement (mGy/mAs)	MCNPX (mGy/mAs)	% Diff.
1	5.90×10^{-03}	5.82×10^{-03}	−1.36	3.69×10^{-02}	3.67×10^{-02}	−0.54
2	7.51×10^{-02}	7.25×10^{-02}	−3.46	1.09×10^{-01}	1.04×10^{-01}	−4.59
3	3.60×10^{-04}	3.47×10^{-04}	−3.61	8.99×10^{-03}	8.90×10^{-02}	−1.00
4	1.52×10^{-03}	1.45×10^{-03}	−4.61	1.53×10^{-02}	1.48×10^{-02}	−3.27
5	6.23×10^{-04}	5.91×10^{-04}	−5.14	2.22×10^{-02}	2.15×10^{-02}	−3.15
Average % Diff. (SD)			−3.64 (1.45)			−2.51 (1.69)

TABLE IV. Comparison of measured and simulated CBCT imaging dose. Each location is referenced from the diagram in Fig. 4.

	Pelvis CBCT			Standard-dose head CBCT		
Location	Measurement (mGy/mAs)	MCNPX (mGy/mAs)	% Diff.	Measurement (mGy/mAs)	MCNPX (mGy/mAs)	% Diff.
1	2.28×10^{-02}	2.23×10^{-02}	−2.19	3.36×10^{-02}	3.22×10^{-02}	−4.17
2	3.82×10^{-02}	3.68×10^{-02}	−3.66	1.13×10^{-02}	1.07×10^{-02}	−5.31
3	3.58×10^{-02}	3.45×10^{-02}	−3.63	4.84×10^{-02}	4.65×10^{-02}	−3.51
4	3.93×10^{-02}	3.77×10^{-02}	−4.07	2.97×10^{-02}	2.93×10^{-02}	−1.35
5	3.80×10^{-02}	3.68×10^{-02}	−3.16	3.82×10^{-02}	3.70×10^{-02}	−3.14
Average % Diff. (SD)			−3.34 (0.72)			−3.50 (1.46)

a statistical uncertainty of less than 1%. Simulations uniformly underestimated measurements by 1.36%–5.14% for the pelvis AP protocol and 0.54%–4.59% for the head AP protocol. The mean percent difference and standard deviation (SD) of the difference between the measurements and simulations was −3.64% (SD = 1.45%) for the pelvis AP protocol and −2.51% (SD = 1.69%) for the head AP protocol.

3.C. CBCT imaging validation

Table IV shows the measured and simulated in-phantom dose for the CBCT imaging protocols. For each simulation, 10×10^6 photons histories were used to achieve a statistical uncertainty of less than 1%. Simulations uniformly underestimated measurements by 2.19%–4.07% for the pelvis CBCT protocol and 1.35%–5.31% for the standard-dose head CBCT protocol. The mean percent difference between the measurements and simulations was −3.34% (SD = 0.72%) for the pelvis CBCT protocol and −3.50% (SD = 1.46%) for the standard-dose head CBCT protocol.

4. DISCUSSION AND CONCLUSIONS

Besides alleviating the need to obtain proprietary data from the manufacturer to construct a Monte Carlo model of the OBI, this measurement-based approach customizes the source specifications to match physical measurements made using the exact machine of interest. Any modifications made to the OBI device or software after factory assembly may not resonate in the manufacturer provided beam characteristics or bowtie profile data. The measurement-based approach, though, will appropriately incorporate any variations into the model.

Because the bowties filters of the OBI kV imaging system integrated into the Varian Novalis Tx radiosurgery platform are shaped in the direction parallel to the anode-cathode direction of the x-ray tube, bowtie profile measurements will be subject to the anode heel effect. The anode heel effect is enhanced in the OBI because of the use of a steeply angled anode as part of a rotating anode tube. It is therefore important that the full profile of each bowtie be measured in its entirety. This is especially true for the full-bowtie filter. In the original measurement-based method developed for conventional CT dose calculation and simulation, only half of the bowtie profile was measured and symmetry was assumed about the central ray because the anode heel effect did not exist in the direction of the profile for all the CT scanners investigated.[16] While manufacturer schematics show that the physical full-bowtie is symmetric about the central ray in the axial plane, the Fig. 8 demonstrates some asymmetry about the central ray for the Al equivalent length bowtie filter description. This is most likely due to the anode heel effect present in the direction of the profile and potentially other machine specific effects on the x-ray beam intensity such as source misalignment. Asymmetry has also been demonstrated by Ding *et al.* in fluence profile simulations using an electrons-on-target OBI source model constructed from manufacturer's data specifications.[12]

In order to understand the potential dose differences that would arise between simulations and measurements if machine specific effects on the x-ray beam's intensity throughout its entirety, such as the anode heel effect, were not modeled within the Al equivalent length bowtie filter description, a symmetric full-bowtie profile was constructed and used within Monte Carlo simulations of the head AP protocol. Figure 9 shows a full-bowtie profile derived from measuring

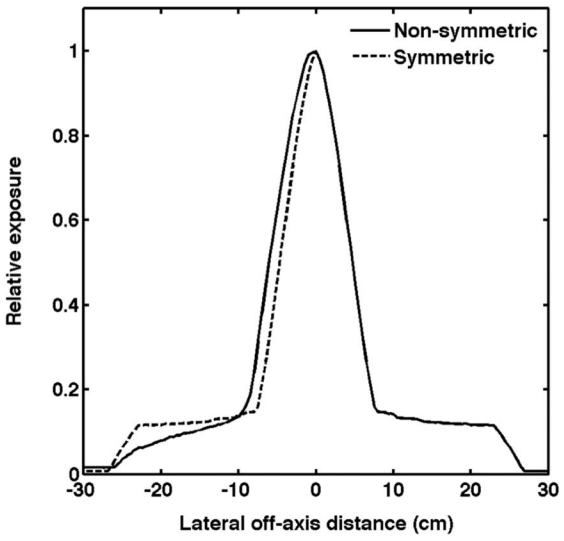

FIG. 9. Symmetric full-bowtie profile and full-bowtie profile measured in its entirety.

TABLE V. Comparison of measured and simulated imaging dose for the head AP protocol using a symmetric full-bowtie profile.

Location	Measurement (mGy/mAs)	MCNPX (mGy/mAs)	% Diff.
1	3.69×10^{-02}	3.57×10^{-02}	−3.25
2	1.09×10^{-01}	1.02×10^{-01}	−6.42
3	8.99×10^{-03}	8.52×10^{-03}	−5.23
4	1.53×10^{-02}	1.46×10^{-02}	−4.58
5	2.22×10^{-02}	1.66×10^{-02}	−25.23
Average % Diff. (SD)			−8.94 (9.18)

half of the bowtie profile and assuming symmetry around the central axis overlaid on the full-bowtie profile measured in its entirety. Clearly there is asymmetry about the axis within the region that would constitute the collimated x-ray beam for the protocol used (See Table II). Table V shows the differences between simulations and measurements if the bowtie profile that assumes symmetry was used within Monte Carlo simulations of the head AP protocol. The difference is most notable at the lateral in-phantom measurement location on the side of the bowtie profile that was assumed to be symmetric. Had machine specific effects on the x-ray beam intensity not been taken into account within the source models used in this investigation, it is reasonable to conclude that simulation results beyond the head AP protocol would not have agreed so nicely with the measurements because of the asymmetry present in the machine used in this study.

In this investigation, an equivalent source model, originally developed for CT dose quantification, has been successfully adapted for use in Monte Carlo simulations of dose from the radiographic and CBCT modes of operation of the OBI. A careful validation has been performed and the results demonstrate the accuracy of this measurement-based approach to reproduce in-phantom measurements for an assortment of technical settings and parameters of the OBI. Protocols utilizing the full- and half-bowtie, a variety of beam energies, the full- and half-fan mode and a full- and partial-scan were all validated using the equivalent source model. Future work will focus on anthropomorphic and patient-specific dose assessment.

ACKNOWLEDGMENTS

The authors would like to acknowledge the contribution of Dr. John DeMarco for establishing the MCNP prototype. The authors also want to thank Dr. Steve Tenn and Mr. Philip Chow for their assistance in clinical setup and experimental measurement. Portions of this research were supported by grants from Siemens Healthcare, the American Association of Cancer Research (AACR) and The Tobacco Related Disease Research Program (TRDRP) from the University of California Office of the President (UCOP).

[a]Author to whom correspondence should be addressed. Electronic mail: kmcmillan@mednet.ucla.edu

[1]M. K. Islam *et al.*, "Patient dose from kilovoltage cone beam computed tomography imaging in radiation therapy," Med. Phys. **33**, 1573–1582 (2006).
[2]N. Wen *et al.*, "Dose delivered from Varian's CBCT to patients receiving IMRT for prostate cancer," Phys. Med. Biol. **52**, 2267–2276 (2007).
[3]M. J. Murphy *et al.*, "The management of imaging dose during image-guided radiotherapy: Report of the AAPM Task Group 75," Med. Phys. **34**, 4041–4063 (2007).
[4]E. G. A. Aird, "Second cancer risk, concomitant exposures, and IRMER(2000)," Br. J. Radiol. **77**, 983–985 (2004).
[5]S. P. Waddington and A. L. McKenzie, "Assessment of effective dose from concomitant exposures required in verification of the target volume in radiotherapy," Br. J. Radiol. **77**, 557–561 (2004).
[6]D. W. O. Rodgers, "Fifty years of Monte Carlo simulations for medical physics," Phys. Med. Biol. **51**, 287–301 (2006).
[7]J. V. Atherton and W. Huda, "CT dose in cylindrical phantoms," Phys. Med. Biol. **40**, 891–911 (1995).
[8]M. Caon *et al.*, "A comparison of radiation dose measured in CT dosimetry phantoms with calculations using EGS4 and voxel-based computational models," Phys. Med. Biol. **42**, 219–229 (1997).
[9]J. M. Boone *et al.*, "Monte Carlo assessment of computed tomography dose to tissue adjacent to the scanned volume," Med. Phys. **27**, 2393–2407 (2000).
[10]G. Jarry *et al.*, "A Monte Carlo-based method to estimate radiation dose from spiral CT: From phantom testing to patient-specific models," Phys. Med. Biol. **48**, 2645–2663 (2003).
[11]P. A. Lucas *et al.*, "Monte Carlo simulations in CT for the study of the surface air kerma and energy imparted to phantoms of varying size and position," Phys. Med. Biol. **49**, 1439–1454 (2004).
[12]G. X. Ding *et al.*, "Characteristics of kilovoltage x-ray beams used for cone-beam computed tomography in radiation therapy," Phys. Med. Biol. **52**, 1595–1615 (2007).
[13]G. X. Ding *et al.*, "Accurate patient dosimetry of kilovoltage cone-beam CT in radiation therapy," Med. Phys. **35**, 1135–1144 (2008).
[14]S. Kim *et al.*, "Kilovoltage cone-beam CT: Comparative dose and image quality evaluations in partial and full-angle scan protocols," Med. Phys. **37**, 3648–3659 (2010).
[15]S. Kim *et al.*, "Computed tomography dose index and dose length product for cone-beam CT: Monte Carlo simulations of a commercial system," J. Appl. Clin. Med. Phys. **12**, 84–95 (2011).
[16]A. C. Turner *et al.*, "A method to generate equivalent energy spectra and filtration models based on measurement for multidetector CT Monte Carlo dosimetry simulations," Med. Phys. **36**, 2154–2164 (2009).
[17]J. M. Boone, "Equivalent spectra as a measure of beam quality," Med. Phys. **13**, 861–868 (1986).
[18]J. H. Siewerdsen *et al.*, "SPEKTR: A computational tool for x-ray spectral analysis and imaging system optimization," Med. Phys. **31**, 3057–3067 (2004).
[19]J. M. Boone and J. A. Seibert, "An accurate method for computer generating tungsten anode x-ray spectra from 30 to 140 kV," Med. Phys. **24**, 1661–1670 (1997).
[20]J. H. Hubbell and S. M. Seltzer, "Tables of x-ray mass attenuation coefficients and mass energy-absorption coefficients" (2004) (available URL: http://physics.nist.gov/PhysRefData/XrayMassCoef/cover.html).
[21]D. B. Pelowitz *et al.*, "MCNPX 2.7.A Extensions," Los Alamos National Laboratory Report LA-UR-08-07182, 2008.
[22]J. H. Hubbell *et al.*, "Atomic form factors, incoherent scattering functions and photon scattering cross sections," J. Phys. Chem. Ref. Data **4**, 471–538 (1975).
[23]J. J. DeMarco *et al.*, "A Monte Carlo based method to estimate radiation dose from multidetector CT (MCDT): Cylindrical and anthropimorphic phantoms," Phys. Med. Biol. **50**, 3989–4004 (2005).
[24]G. Zhang *et al.*, "Monte Carlo modeling for dose assessment in cone beam CT for oral and maxillofacial applications," Med. Phys. **40**, 072103 (12pp.) (2013).